All-sky search for gravitational-wave bursts in the second joint LIGO-Virgo run

J. Abadie, B. P. Abbott, R. Abbott, T. D. Abbott, M. Abernathy, T. Accadia, F. Acernese, C. Adams, R. Adhikari, C. Affeldt, et al.

All-sky search for gravitational-wave bursts in the second joint LIGO-Virgo run

J. Abadie,[1,z] B. P. Abbott,[1,z] R. Abbott,[1,z] T. D. Abbott,[2,z] M. Abernathy,[3,z] T. Accadia,[4,z] F. Acernese,[5a,5c,z] C. Adams,[6,z] R. Adhikari,[1,z] C. Affeldt,[7,8,z] M. Agathos,[9a,z] K. Agatsuma,[10,z] P. Ajith,[1,z] B. Allen,[7,11,8,z] E. Amador Ceron,[11,z] D. Amariutei,[12,z] S. B. Anderson,[1,z] W. G. Anderson,[11,z] K. Arai,[1,z] M. A. Arain,[12,z] M. C. Araya,[1,z] S. M. Aston,[13,z] P. Astone,[14a,z] D. Atkinson,[15,z] P. Aufmuth,[8,7,z] C. Aulbert,[7,8,z] B. E. Aylott,[13,z] S. Babak,[16,z] P. Baker,[17,z] G. Ballardin,[18,z] S. Ballmer,[19,z] J. C. B. Barayoga,[1,z] D. Barker,[15,z] F. Barone,[5a,5c,z] B. Barr,[3,z] L. Barsotti,[20,z] M. Barsuglia,[21,z] M. A. Barton,[15,z] I. Bartos,[22,z] R. Bassiri,[3,z] M. Bastarrika,[3,z] A. Basti,[23a,23b,z] J. Batch,[15,z] J. Bauchrowitz,[7,8,z] Th. S. Bauer,[9a,z] M. Bebronne,[4,z] D. Beck,[24,z] B. Behnke,[16,z] M. Bejger,[25c,z] M. G. Beker,[9a,z] A. S. Bell,[3,z] A. Belletoile,[4,z] I. Belopolski,[22,z] M. Benacquista,[26,z] J. M. Berliner,[15,z] A. Bertolini,[7,8,z] J. Betzwieser,[1,z] N. Beveridge,[3,z] P. T. Beyersdorf,[27,z] I. A. Bilenko,[28,z] G. Billingsley,[1,z] J. Birch,[6,z] R. Biswas,[26,z] M. Bitossi,[23a,z] M. A. Bizouard,[29a,z] E. Black,[1,z] J. K. Blackburn,[1,z] L. Blackburn,[30,z] D. Blair,[31,z] B. Bland,[15,z] M. Blom,[9a,z] O. Bock,[7,8,z] T. P. Bodiya,[20,z] C. Bogan,[7,8,z] R. Bondarescu,[32,z] F. Bondu,[33b,z] L. Bonelli,[23a,23b,z] R. Bonnand,[34,z] R. Bork,[1,z] M. Born,[7,8,z] V. Boschi,[23a,z] S. Bose,[35,z] L. Bosi,[36a,z] B. Bouhou,[21,z] S. Braccini,[23a,z] C. Bradaschia,[23a,z] P. R. Brady,[11,z] V. B. Braginsky,[28,z] M. Branchesi,[37a,37b,z] J. E. Brau,[38,z] J. Breyer,[7,8,z] T. Briant,[39,z] D. O. Bridges,[6,z] A. Brillet,[33a,z] M. Brinkmann,[7,8,z] V. Brisson,[29a,z] M. Britzger,[7,8,z] A. F. Brooks,[1,z] D. A. Brown,[19,z] T. Bulik,[25b,z] H. J. Bulten,[9a,9b,z] A. Buonanno,[40,z] J. Burguet–Castell,[41,z] D. Buskulic,[4,z] C. Buy,[21,z] R. L. Byer,[24,z] L. Cadonati,[42,z] G. Cagnoli,[37a,z] E. Calloni,[5a,5b,z] J. B. Camp,[30,z] P. Campsie,[3,z] J. Cannizzo,[30,z] K. Cannon,[43,z] B. Canuel,[18,z] J. Cao,[44,z] C. D. Capano,[19,z] F. Carbognani,[18,z] L. Carbone,[13,z] S. Caride,[45,z] S. Caudill,[46,z] M. Cavaglià,[47,z] F. Cavalier,[29a,z] R. Cavalieri,[18,z] G. Cella,[23a,z] C. Cepeda,[1,z] E. Cesarini,[37b,z] O. Chaibi,[33a,z] T. Chalermsongsak,[1,z] P. Charlton,[48,z] E. Chassande-Mottin,[21,z] S. Chelkowski,[13,z] W. Chen,[44,z] X. Chen,[31,z] Y. Chen,[49,z] A. Chincarini,[50,z] A. Chiummo,[18,z] H. S. Cho,[51,z] J. Chow,[52,z] N. Christensen,[53,z] S. S. Y. Chua,[52,z] C. T. Y. Chung,[54,z] S. Chung,[31,z] G. Ciani,[12,z] F. Clara,[15,z] D. E. Clark,[24,z] J. Clark,[55,z] J. H. Clayton,[11,z] F. Cleva,[33a,z] E. Coccia,[56a,56b,z] P.-F. Cohadon,[39,z] C. N. Colacino,[23a,23b,z] J. Colas,[18,z] A. Colla,[14a,14b,z] M. Colombini,[14b,z] A. Conte,[14a,14b,z] R. Conte,[57,z] D. Cook,[15,z] T. R. Corbitt,[20,z] M. Cordier,[27,z] N. Cornish,[17,z] A. Corsi,[1,z] C. A. Costa,[46,z] M. Coughlin,[53,z] J.-P. Coulon,[33a,z] P. Couvares,[19,z] D. M. Coward,[31,z] M. Cowart,[6,z] D. C. Coyne,[1,z] J. D. E. Creighton,[11,z] T. D. Creighton,[26,z] A. M. Cruise,[13,z] A. Cumming,[3,z] L. Cunningham,[3,z] E. Cuoco,[18,z] R. M. Cutler,[13,z] K. Dahl,[7,8,z] S. L. Danilishin,[28,z] R. Dannenberg,[1,z] S. D'Antonio,[56a,z] K. Danzmann,[7,8,z] V. Dattilo,[18,z] B. Daudert,[1,z] H. Daveloza,[26,z] M. Davier,[29a,z] E. J. Daw,[58,z] R. Day,[18,z] T. Dayanga,[35,z] R. De Rosa,[5a,5b,z] D. DeBra,[24,z] G. Debreczeni,[59,z] W. Del Pozzo,[9a,z] M. del Prete,[60b,z] T. Dent,[55,z] V. Dergachev,[1,z] R. DeRosa,[46,z] R. DeSalvo,[1,z] S. Dhurandhar,[61,z] L. Di Fiore,[5a,z] A. Di Lieto,[23a,23b,z] I. Di Palma,[7,8,z] M. Di Paolo Emilio,[56a,56c,z] A. Di Virgilio,[23a,z] M. Díaz,[26,z] A. Dietz,[4,z] F. Donovan,[20,z] K. L. Dooley,[12,z] M. Drago,[60a,60b,z] R. W. P. Drever,[62,z] J. C. Driggers,[1,z] Z. Du,[44,z] J.-C. Dumas,[31,z] S. Dwyer,[20,z] T. Eberle,[7,8,z] M. Edgar,[3,z] M. Edwards,[55,z] A. Effler,[46,z] P. Ehrens,[1,z] G. Endrőczi,[59,z] R. Engel,[1,z] T. Etzel,[1,z] K. Evans,[3,z] M. Evans,[20,z] T. Evans,[6,z] M. Factourovich,[22,z] V. Fafone,[56a,56b,z] S. Fairhurst,[55,z] Y. Fan,[31,z] B. F. Farr,[63,z] D. Fazi,[63,z] H. Fehrmann,[7,8,z] D. Feldbaum,[12,z] F. Feroz,[64,z] I. Ferrante,[23a,23b,z] F. Fidecaro,[23a,23b,z] L. S. Finn,[32,z] I. Fiori,[18,z] R. P. Fisher,[32,z] R. Flaminio,[34,z] M. Flanigan,[15,z] S. Foley,[20,z] E. Forsi,[6,z] L. A. Forte,[5a,z] N. Fotopoulos,[1,z] J.-D. Fournier,[33a,z] J. Franc,[34,z] S. Frasca,[14a,14b,z] F. Frasconi,[23a,z] M. Frede,[7,8,z] M. Frei,[65,66,z] Z. Frei,[67,z] A. Freise,[13,z] R. Frey,[38,z] T. T. Fricke,[46,z] D. Friedrich,[7,8,z] P. Fritschel,[20,z] V. V. Frolov,[6,z] M.-K. Fujimoto,[10,z] P. J. Fulda,[13,z] M. Fyffe,[6,z] J. Gair,[64,z] M. Galimberti,[34,z] L. Gammaitoni,[36a,36b,z] J. Garcia,[15,z] F. Garufi,[5a,5b,z] M. E. Gáspár,[59,z] G. Gemme,[50,z] R. Geng,[44,z] E. Genin,[18,z] A. Gennai,[23a,z] L. Á. Gergely,[68,z] S. Ghosh,[35,z] J. A. Giaime,[46,6,z] S. Giampanis,[11,z] K. D. Giardina,[6,z] A. Giazotto,[23a,z] S. Gil-Casanova,[41,z] C. Gill,[3,z] J. Gleason,[12,z] E. Goetz,[7,8,z] L. M. Goggin,[11,z] G. González,[46,z] M. L. Gorodetsky,[28,z] S. Goßler,[7,8,z] R. Gouaty,[4,z] C. Graef,[7,8,z] P. B. Graff,[64,z] M. Granata,[21,z] A. Grant,[3,z] S. Gras,[31,z] C. Gray,[15,z] N. Gray,[3,z] R. J. S. Greenhalgh,[69,z] A. M. Gretarsson,[70,z] C. Greverie,[33a,z] R. Grosso,[26,z] H. Grote,[7,8,z] S. Grunewald,[16,z] G. M. Guidi,[37a,37b,z] C. Guido,[6,z] R. Gupta,[61,z] E. K. Gustafson,[1,z] R. Gustafson,[45,z] T. Ha,[71,z] J. M. Hallam,[13,z] D. Hammer,[11,z] G. Hammond,[3,z] J. Hanks,[15,z] C. Hanna,[1,72,z] J. Hanson,[6,z] J. Harms,[62,z] A. Hardt,[53] G. M. Harry,[20,z] I. W. Harry,[55,z] E. D. Harstad,[38,z] M. T. Hartman,[12,z] K. Haughian,[3,z] K. Hayama,[10,z] J.-F. Hayau,[33b,z] J. Heefner,[1,z] A. Heidmann,[39,z] M. C. Heintze,[12,z] H. Heitmann,[33a,z] P. Hello,[29a,z] M. A. Hendry,[3,z] I. S. Heng,[3,z] A. W. Heptonstall,[1,z] V. Herrera,[24,z] M. Hewitson,[7,8,z] S. Hild,[3,z] D. Hoak,[42,z] K. A. Hodge,[1,z] K. Holt,[6,z] M. Holtrop,[73,z] T. Hong,[49,z] S. Hooper,[31,z] D. J. Hosken,[74,z] J. Hough,[3,z] E. J. Howell,[31,z] B. Hughey,[11,z] S. Husa,[41,z] S. H. Huttner,[3,z] T. Huynh-Dinh,[6,z] D. R. Ingram,[15,z] R. Inta,[52,z] T. Isogai,[53,z] A. Ivanov,[1,z] K. Izumi,[10,z] M. Jacobson,[1,z] E. James,[1,z] Y. J. Jang,[43,z] P. Jaranowski,[25d,z] E. Jesse,[70,z] W. W. Johnson,[46,z] D. I. Jones,[75,z] G. Jones,[55,z] R. Jones,[3,z] L. Ju,[31,z] P. Kalmus,[1,z] V. Kalogera,[63,z] S. Kandhasamy,[76,z] G. Kang,[77,z] J. B. Kanner,[40,z] R. Kasturi,[78,z]

E. Katsavounidis,[20,z] W. Katzman,[6,z] H. Kaufer,[7,8,z] K. Kawabe,[15,z] S. Kawamura,[10,z] F. Kawazoe,[7,8,z] D. Kelley,[19,z] W. Kells,[1,z] D. G. Keppel,[1,z] Z. Keresztes,[68,z] A. Khalaidovski,[7,8,z] F. Y. Khalili,[28,z] E. A. Khazanov,[79,z] B. K. Kim,[77,z] C. Kim,[80,z] H. Kim,[7,8,z] K. Kim,[81,z] N. Kim,[24,z] Y. M. Kim,[51,z] P. J. King,[1,z] D. L. Kinzel,[6,z] J. S. Kissel,[20,z] S. Klimenko,[12,z] K. Kokeyama,[13,z] V. Kondrashov,[1,z] S. Koranda,[11,z] W. Z. Korth,[1,z] I. Kowalska,[25b,z] D. Kozak,[1,z] O. Kranz,[7,8,z] V. Kringel,[7,8,z] S. Krishnamurthy,[63,z] B. Krishnan,[16,z] A. Królak,[25a,25e,z] G. Kuehn,[7,8,z] R. Kumar,[3,z] P. Kwee,[8,7,z] P. K. Lam,[52,z] M. Landry,[15,z] B. Lantz,[24,z] N. Lastzka,[7,8,z] C. Lawrie,[3,z] A. Lazzarini,[1,z] P. Leaci,[16,z] C. H. Lee,[51,z] H. K. Lee,[81,z] H. M. Lee,[82,z] J. R. Leong,[7,8,z] I. Leonor,[38,z] N. Leroy,[29a,z] N. Letendre,[4,z] J. Li,[44,z] T. G. F. Li,[9a,z] N. Liguori,[60a,60b,z] P. E. Lindquist,[1,z] Y. Liu,[44,z] Z. Liu,[12,z] N. A. Lockerbie,[83,z] D. Lodhia,[13,z] M. Lorenzini,[37a,z] V. Loriette,[29b,z] M. Lormand,[6,z] G. Losurdo,[37a,z] J. Lough,[19,z] J. Luan,[49,z] M. Lubinski,[15,z] H. Lück,[7,8,z] A. P. Lundgren,[32,z] E. Macdonald,[3,z] B. Machenschalk,[7,8,z] M. MacInnis,[20,z] D. M. Macleod,[55,z] M. Mageswaran,[1,z] K. Mailand,[1,z] E. Majorana,[14a,z] I. Maksimovic,[29b,z] N. Man,[33a,z] I. Mandel,[20,13,z] V. Mandic,[76,z] M. Mantovani,[23a,23c,z] A. Marandi,[24,z] F. Marchesoni,[36a,z] F. Marion,[4,z] S. Márka,[22,z] Z. Márka,[22,z] A. Markosyan,[24,z] E. Maros,[1,z] J. Marque,[18,z] F. Martelli,[37a,37b,z] I. W. Martin,[3,z] R. M. Martin,[12,z] J. N. Marx,[1,z] K. Mason,[20,z] A. Masserot,[4,z] F. Matichard,[20,z] L. Matone,[22,z] R. A. Matzner,[65,z] N. Mavalvala,[20,z] G. Mazzolo,[7,8,z] R. McCarthy,[15,z] D. E. McClelland,[52,z] S. C. McGuire,[84,z] G. McIntyre,[1,z] J. McIver,[42,z] D. J. A. McKechan,[55,z] S. McWilliams,[22,z] G. D. Meadors,[45,z] M. Mehmet,[7,8,z] T. Meier,[8,7,z] A. Melatos,[54,z] A. C. Melissinos,[85,z] G. Mendell,[15,z] R. A. Mercer,[11,z] S. Meshkov,[1,z] C. Messenger,[55,z] M. S. Meyer,[6,z] H. Miao,[49,z] C. Michel,[34,z] L. Milano,[5a,5b,z] J. Miller,[52,z] Y. Minenkov,[56a,z] V. P. Mitrofanov,[28,z] G. Mitselmakher,[12,z] R. Mittleman,[20,z] O. Miyakawa,[10,z] B. Moe,[11,z] M. Mohan,[18,z] S. D. Mohanty,[26,z] S. R. P. Mohapatra,[42,z] D. Moraru,[15,z] G. Moreno,[15,z] N. Morgado,[34,z] A. Morgia,[56a,56b,z] T. Mori,[10,z] S. R. Morriss,[26,z] S. Mosca,[5a,5b,z] K. Mossavi,[7,8,z] B. Mours,[4,z] C. M. Mow–Lowry,[52,z] C. L. Mueller,[12,z] G. Mueller,[12,z] S. Mukherjee,[26,z] A. Mullavey,[52,z] H. Müller-Ebhardt,[7,8,z] J. Munch,[74,z] D. Murphy,[22,z] P. G. Murray,[3,z] A. Mytidis,[12,z] T. Nash,[1,z] L. Naticchioni,[14a,14b,z] V. Necula,[12,z] J. Nelson,[3,z] I. Neri,[36a,36b,z] G. Newton,[3,z] T. Nguyen,[52,z] A. Nishizawa,[10,z] A. Nitz,[19,z] F. Nocera,[18,z] D. Nolting,[6,z] M. E. Normandin,[26,z] L. Nuttall,[55,z] E. Ochsner,[11,z] J. O'Dell,[69,z] E. Oelker,[20,z] G. H. Ogin,[1,z] J. J. Oh,[71,z] S. H. Oh,[71,z] B. O'Reilly,[6,z] R. O'Shaughnessy,[11,z] C. Osthelder,[1,z] C. D. Ott,[49,z] D. J. Ottaway,[74,z] R. S. Ottens,[12,z] H. Overmier,[6,z] B. J. Owen,[32,z] A. Page,[13,z] G. Pagliaroli,[56a,56c,z] L. Palladino,[56a,56c,z] C. Palomba,[14a,z] Y. Pan,[40,z] C. Pankow,[12,z] F. Paoletti,[23a,18,z] M. A. Papa,[16,11,z] M. Parisi,[5a,5b,z] A. Pasqualetti,[18,z] R. Passaquieti,[23a,23b,z] D. Passuello,[23a,z] P. Patel,[1,z] M. Pedraza,[1,z] P. Peiris,[66,z] L. Pekowsky,[19,z] S. Penn,[78,z] A. Perreca,[19,z] G. Persichetti,[5a,5b,z] M. Phelps,[1,z] M. Pichot,[33a,z] M. Pickenpack,[7,8,z] F. Piergiovanni,[37a,37b,z] M. Pietka,[25d,z] L. Pinard,[34,z] I. M. Pinto,[86,z] M. Pitkin,[3,z] H. J. Pletsch,[7,8,z] M. V. Plissi,[3,z] R. Poggiani,[23a,23b,z] J. Pöld,[7,8,z] F. Postiglione,[57,z] M. Prato,[50,z] V. Predoi,[55,z] T. Prestegard,[76,z] L. R. Price,[1,z] M. Prijatelj,[7,8,z] M. Principe,[86,z] S. Privitera,[1,z] R. Prix,[7,8,z] G. A. Prodi,[60a,60b,z] L. G. Prokhorov,[28,z] O. Puncken,[7,8,z] M. Punturo,[36a,z] P. Puppo,[14a,z] V. Quetschke,[26,z] R. Quitzow-James,[38,z] F. J. Raab,[15,z] D. S. Rabeling,[9a,9b,z] I. Rácz,[59,z] H. Radkins,[15,z] P. Raffai,[67,z] M. Rakhmanov,[26,z] B. Rankins,[47,z] P. Rapagnani,[14a,14b,z] V. Raymond,[63,z] V. Re,[56a,56b,z] K. Redwine,[22,z] C. M. Reed,[15,z] T. Reed,[87,z] T. Regimbau,[33a,z] S. Reid,[3,z] D. H. Reitze,[12,z] F. Ricci,[14a,14b,z] R. Riesen,[6,z] K. Riles,[45,z] N. A. Robertson,[1,3,z] F. Robinet,[29a,z] C. Robinson,[55,z] E. L. Robinson,[16,z] A. Rocchi,[56a,z] S. Roddy,[6,z] C. Rodriguez,[63,z] M. Rodruck,[15,z] L. Rolland,[4,z] J. G. Rollins,[1,z] J. D. Romano,[26,z] R. Romano,[5a,5c,z] J. H. Romie,[6,z] D. Rosińska,[25d,25f,z] C. Röver,[7,8,z] S. Rowan,[3,z] A. Rüdiger,[7,8,z] P. Ruggi,[18,z] K. Ryan,[15,z] P. Sainathan,[12,z] F. Salemi,[7,8,z] L. Sammut,[54,z] V. Sandberg,[15,z] V. Sannibale,[1,z] L. Santamaría,[1,z] I. Santiago-Prieto,[3,z] G. Santostasi,[88,z] B. Sassolas,[34,z] B. S. Sathyaprakash,[55,z] S. Sato,[10,z] P. R. Saulson,[19,z] R. L. Savage,[15,z] R. Schilling,[7,8,z] R. Schnabel,[7,8,z] R. M. S. Schofield,[38,z] E. Schreiber,[7,8,z] B. Schulz,[7,8,z] B. F. Schutz,[16,55,z] P. Schwinberg,[15,z] J. Scott,[3,z] S. M. Scott,[52,z] F. Seifert,[1,z] D. Sellers,[6,z] D. Sentenac,[18,z] A. Sergeev,[79,z] D. A. Shaddock,[52,z] M. Shaltev,[7,8,z] B. Shapiro,[20,z] P. Shawhan,[40,z] D. H. Shoemaker,[20,z] A. Sibley,[6,z] X. Siemens,[11,z] D. Sigg,[15,z] A. Singer,[1,z] L. Singer,[1,z] A. M. Sintes,[41,z] G. R. Skelton,[11,z] B. J. J. Slagmolen,[52,z] J. Slutsky,[46,z] J. R. Smith,[2,z] M. R. Smith,[1,z] R. J. E. Smith,[13,z] N. D. Smith-Lefebvre,[15,z] K. Somiya,[49,z] B. Sorazu,[3,z] J. Soto,[20,z] F. C. Speirits,[3,z] L. Sperandio,[56a,56b,z] M. Stefszky,[52,z] A. J. Stein,[20,z] L. C. Stein,[20,z] E. Steinert,[15,z] J. Steinlechner,[7,8,z] S. Steinlechner,[7,8,z] S. Steplewski,[35,z] A. Stochino,[1,z] R. Stone,[26,z] K. A. Strain,[3,z] S. E. Strigin,[28,z] A. S. Stroeer,[26,z] R. Sturani,[37a,37b,z] A. L. Stuver,[6,z] T. Z. Summerscales,[89,z] M. Sung,[46,z] S. Susmithan,[31,z] P. J. Sutton,[55,z] B. Swinkels,[18,z] M. Tacca,[18,z] L. Taffarello,[60c,z] D. Talukder,[35,z] D. B. Tanner,[12,z] S. P. Tarabrin,[7,8,z] J. R. Taylor,[7,8,z] R. Taylor,[1,z] P. Thomas,[15,z] K. A. Thorne,[6,z] K. S. Thorne,[49,z] E. Thrane,[76,z] A. Thüring,[8,7,z] K. V. Tokmakov,[83,z] C. Tomlinson,[58,z] A. Toncelli,[23a,23b,z] M. Tonelli,[23a,23b,z] O. Torre,[23a,23c,z] C. Torres,[6,z] C. I. Torrie,[1,3,z] E. Tournefier,[4,z] F. Travasso,[36a,36b,z] G. Traylor,[6,z] K. Tseng,[24,z] E. Tucker,[53] D. Ugolini,[90,z] H. Vahlbruch,[8,7,z] G. Vajente,[23a,23b,z] J. F. J. van den Brand,[9a,9b,z] C. Van Den Broeck,[9a,z] S. van der Putten,[9a,z] A. A. van Veggel,[3,z] S. Vass,[1,z] M. Vasuth,[59,z] R. Vaulin,[20,z] M. Vavoulidis,[29a,z] A. Vecchio,[13,z]

G. Vedovato,[60c,z] J. Veitch,[55,z] P. J. Veitch,[74,z] C. Veltkamp,[7,8,z] D. Verkindt,[4,z] F. Vetrano,[37a,37b,z] A. Viceré,[37a,37b,z] A. E. Villar,[1,z] J.-Y. Vinet,[33a,z] S. Vitale,[70,9a,z] H. Vocca,[36a,z] C. Vorvick,[15,z] S. P. Vyatchanin,[28,z] A. Wade,[52,z] L. Wade,[11,z] M. Wade,[11,z] S. J. Waldman,[20,z] L. Wallace,[1,z] Y. Wan,[44,z] M. Wang,[13,z] X. Wang,[44,z] Z. Wang,[44,z] A. Wanner,[7,8,z] R. L. Ward,[21,z] M. Was,[29a,z] M. Weinert,[7,8,z] A. J. Weinstein,[1,z] R. Weiss,[20,z] L. Wen,[49,31,z] P. Wessels,[7,8,z] M. West,[19,z] T. Westphal,[7,8,z] K. Wette,[7,8,z] J. T. Whelan,[66,z] S. E. Whitcomb,[1,31,z] D. J. White,[58,z] B. F. Whiting,[12,z] C. Wilkinson,[15,z] P. A. Willems,[1,z] L. Williams,[12,z] R. Williams,[1,z] B. Willke,[7,8,z] L. Winkelmann,[7,8,z] W. Winkler,[7,8,z] C. C. Wipf,[20,z] A. G. Wiseman,[11,z] H. Wittel,[7,8,z] G. Woan,[3,z] R. Wooley,[6,z] J. Worden,[15,z] I. Yakushin,[6,z] H. Yamamoto,[1,z] K. Yamamoto,[7,8,60b,60d,z] C. C. Yancey,[40,z] H. Yang,[49,z] D. Yeaton-Massey,[1,z] S. Yoshida,[91,z] P. Yu,[11,z] M. Yvert,[4,z] A. Zadrożny,[25e,z] M. Zanolin,[70,z] J.-P. Zendri,[60c,z] F. Zhang,[44,z] L. Zhang,[1,z] W. Zhang,[44,z] C. Zhao,[31,z] N. Zotov,[87,z] M. E. Zucker,[20,z] and J. Zweizig[1,z]

(*The LIGO Scientific Collaboration)
([†]The Virgo Collaboration)

[1]*LIGO - California Institute of Technology, Pasadena, California 91125, USA*
[2]*California State University Fullerton, Fullerton California 92831 USA*
[3]*SUPA, University of Glasgow, Glasgow, G12 8QQ, United Kingdom*
[4]*Laboratoire d'Annecy-le-Vieux de Physique des Particules (LAPP), Université de Savoie, CNRS/IN2P3, F-74941 Annecy-Le-Vieux, France*
[5a]*INFN, Sezione di Napoli, I-84084 Salerno, Italy*
[5b]*Università di Napoli 'Federico II', Complesso Universitario di Monte S. Angelo, I-80126 Napoli, I-84084 Salerno, Italy*
[5c]*Università di Salerno, Fisciano, I-84084 Salerno, Italy*
[6]*LIGO - Livingston Observatory, Livingston, Louisiana 70754, USA*
[7]*Albert-Einstein-Institut, Max-Planck-Institut für Gravitationsphysik, D-30167 Hannover, Germany*
[8]*Leibniz Universität Hannover, D-30167 Hannover, Germany*
[9a]*Nikhef, Science Park, Amsterdam, the Netherlands, 1081 HV Amsterdam, the Netherlands*
[9b]*VU University Amsterdam, De Boelelaan 1081, 1081 HV Amsterdam, the Netherlands*
[10]*National Astronomical Observatory of Japan, Tokyo 181-8588, Japan*
[11]*University of Wisconsin–Milwaukee, Milwaukee, Wisconsin 53201, USA*
[12]*University of Florida, Gainesville, Florida 32611, USA*
[13]*University of Birmingham, Birmingham, B15 2TT, United Kingdom*
[14a]*INFN, Sezione di Roma, I-00185 Roma, Italy*
[14b]*Università 'La Sapienza', I-00185 Roma, Italy*
[15]*LIGO - Hanford Observatory, Richland, Washington 99352, USA*
[16]*Albert-Einstein-Institut, Max-Planck-Institut für Gravitationsphysik, D-14476 Golm, Germany*
[17]*Montana State University, Bozeman, Montana 59717, USA*
[18]*European Gravitational Observatory (EGO), I-56021 Cascina (PI), Italy*
[19]*Syracuse University, Syracuse, New York 13244, USA*
[20]*LIGO - Massachusetts Institute of Technology, Cambridge, Massachusetts 02139, USA*
[21]*APC, AstroParticule et Cosmologie, Université Paris Diderot, CNRS/IN2P3, CEA/Irfu, Observatoire de Paris, Sorbonne Paris Cité, 10, rue Alice Domon et Léonie Duquet, 75205 Paris Cedex 13, France*
[22]*Columbia University, New York, New York 10027, USA*
[23a]*INFN, Sezione di Pisa, I-53100 Siena, Italy*
[23b]*Università di Pisa; I-56127 Pisa, I-53100 Siena, Italy*
[23c]*Università di Siena, I-53100 Siena, Italy*
[24]*Stanford University, Stanford, California 94305, USA*
[25a]*IM-PAN 00-956 Warsaw, Poland*
[25b]*Astronomical Observatory Warsaw University, 00-478 Warsaw, Poland*
[25c]*CAMK-PAN, 00-716 Warsaw, Poland*
[25d]*Białystok University, 15-424 Białystok, Poland*
[25e]*NCBJ, 05-400 Świerk-Otwock, Poland*
[25f]*Institute of Astronomy, 65-265 Zielona Góra, Poland*
[26]*The University of Texas at Brownsville and Texas Southmost College, Brownsville, Texas 78520, USA*
[27]*San Jose State University, San Jose, California 95192, USA*
[28]*Moscow State University, Moscow, 119992, Russia*
[29a]*LAL, Université Paris-Sud, IN2P3/CNRS, F-91898 Orsay, France*
[29b]*ESPCI, CNRS, F-75005 Paris, France*
[30]*NASA/Goddard Space Flight Center, Greenbelt, Maryland 20771, USA*

[31]*University of Western Australia, Crawley, WA 6009, Australia*
[32]*The Pennsylvania State University, University Park, Pennsylvania 16802, USA*
[33a]*Université Nice-Sophia-Antipolis, CNRS, Observatoire de la Côte d'Azur, F-06304 Nice, France*
[33b]*Institut de Physique de Rennes, CNRS, Université de Rennes 1, 35042 Rennes, France*
[34]*Laboratoire des Matériaux Avancés (LMA), IN2P3/CNRS, F-69622 Villeurbanne, Lyon, France*
[35]*Washington State University, Pullman, Washington 99164, USA*
[36a]*INFN, Sezione di Perugia, I-06123 Perugia, Italy*
[36b]*Università di Perugia, I-06123 Perugia, Italy*
[37a]*INFN, Sezione di Firenze, I-50019 Sesto Fiorentino, Italy*
[37b]*Università degli Studi di Urbino 'Carlo Bo', I-61029 Urbino, Italy*
[38]*University of Oregon, Eugene, Oregon 97403, USA*
[39]*Laboratoire Kastler Brossel, ENS, CNRS, UPMC, Université Pierre et Marie Curie, 4 Place Jussieu, F-75005 Paris, France*
[40]*University of Maryland, College Park, Maryland 20742 USA*
[41]*Universitat de les Illes Balears, E-07122 Palma de Mallorca, Spain*
[42]*University of Massachusetts - Amherst, Amherst, Massachusetts 01003, USA*
[43]*Canadian Institute for Theoretical Astrophysics, University of Toronto, Toronto, Ontario, M5S 3H8, Canada*
[44]*Tsinghua University, Beijing 100084 China*
[45]*University of Michigan, Ann Arbor, Michigan 48109, USA*
[46]*Louisiana State University, Baton Rouge, Louisiana 70803, USA*
[47]*The University of Mississippi, University, Mississippi 38677, USA*
[48]*Charles Sturt University, Wagga Wagga, NSW 2678, Australia*
[49]*Caltech-CaRT, Pasadena, California 91125, USA*
[50]*INFN, Sezione di Genova, I-16146 Genova, Italy*
[51]*Pusan National University, Busan 609-735, Korea*
[52]*Australian National University, Canberra, ACT 0200, Australia*
[53]*Carleton College, Northfield, Minnesota 55057, USA*
[54]*The University of Melbourne, Parkville, VIC 3010, Australia*
[55]*Cardiff University, Cardiff, CF24 3AA, United Kingdom*
[56a]*INFN, Sezione di Roma Tor Vergata, Italy*
[56b]*Università di Roma Tor Vergata, I-00133 Roma, Italy*
[56c]*Università dell'Aquila, I-67100 L'Aquila, Italy*
[57]*University of Salerno, I-84084 Fisciano (Salerno), Italy and INFN (Sezione di Napoli), Italy*
[58]*The University of Sheffield, Sheffield S10 2TN, United Kingdom*
[59]*WIGNER RCP, RMKI, H-1121 Budapest, Konkoly Thege Miklós út 29-33, Hungary*
[60a]*INFN, Gruppo Collegato di Trento, I-38050 Povo, Trento, Italy*
[60b]*Università di Trento, I-38050 Povo, Trento, Italy*
[60c]*INFN, Sezione di Padova, I-35131 Padova, Italy*
[60d]*Università di Padova, I-35131 Padova, Italy*
[61]*Inter-University Centre for Astronomy and Astrophysics, Pune - 411007, India*
[62]*California Institute of Technology, Pasadena, California 91125, USA*
[63]*Northwestern University, Evanston, Illinois 60208, USA*
[64]*University of Cambridge, Cambridge, CB2 1TN, United Kingdom*
[65]*The University of Texas at Austin, Austin, Texas 78712, USA*
[66]*Rochester Institute of Technology, Rochester, New York 14623, USA*
[67]*Eötvös Loránd University, Budapest, 1117 Hungary*
[68]*University of Szeged, 6720 Szeged, Dóm tér 9, Hungary*
[69]*Rutherford Appleton Laboratory, HSIC, Chilton, Didcot, Oxon OX11 0QX United Kingdom*
[70]*Embry-Riddle Aeronautical University, Prescott, Arizona 86301 USA*
[71]*National Institute for Mathematical Sciences, Daejeon 305-390, Korea*
[72]*Perimeter Institute for Theoretical Physics, Ontario, N2L 2Y5, Canada*
[73]*University of New Hampshire, Durham, New Hampshire 03824, USA*
[74]*University of Adelaide, Adelaide, SA 5005, Australia*
[75]*University of Southampton, Southampton, SO17 1BJ, United Kingdom*
[76]*University of Minnesota, Minneapolis, Minnesota 55455, USA*
[77]*Korea Institute of Science and Technology Information, Daejeon 305-806, Korea*
[78]*Hobart and William Smith Colleges, Geneva, New York 14456, USA*
[79]*Institute of Applied Physics, Nizhny Novgorod, 603950, Russia*
[80]*Lund Observatory, Box 43, SE-221 00, Lund, Sweden*
[81]*Hanyang University, Seoul 133-791, Korea*
[82]*Seoul National University, Seoul 151-742, Korea*
[83]*University of Strathclyde, Glasgow, G1 1XQ, United Kingdom*

[84]Southern University and A&M College, Baton Rouge, Louisiana 70813, USA
[85]University of Rochester, Rochester, New York 14627, USA
[86]University of Sannio at Benevento, I-82100 Benevento, Italy and INFN (Sezione di Napoli), Italy
[87]Louisiana Tech University, Ruston, Louisiana 71272, USA
[88]McNeese State University, Lake Charles, Louisiana 70609 USA
[89]Andrews University, Berrien Springs, Michigan 49104 USA
[90]Trinity University, San Antonio, Texas 78212, USA
[91]Southeastern Louisiana University, Hammond, Louisiana 70402, USA
(Received 5 March 2012; published 20 June 2012)

We present results from a search for gravitational-wave bursts in the data collected by the LIGO and Virgo detectors between July 7, 2009 and October 20, 2010: data are analyzed when at least two of the three LIGO-Virgo detectors are in coincident operation, with a total observation time of 207 days. The analysis searches for transients of duration $\lesssim 1$ s over the frequency band 64–5000 Hz, without other assumptions on the signal waveform, polarization, direction or occurrence time. All identified events are consistent with the expected accidental background. We set frequentist upper limits on the rate of gravitational-wave bursts by combining this search with the previous LIGO-Virgo search on the data collected between November 2005 and October 2007. The upper limit on the rate of strong gravitational-wave bursts at the Earth is 1.3 events per year at 90% confidence. We also present upper limits on source rate density per year and Mpc^3 for sample populations of standard-candle sources. As in the previous joint run, typical sensitivities of the search in terms of the root-sum-squared strain amplitude for these waveforms lie in the range $\sim 5 \times 10^{-22}\ \mathrm{Hz}^{-1/2}$ to $\sim 1 \times 10^{-20}\ \mathrm{Hz}^{-1/2}$. The combination of the two joint runs entails the most sensitive all-sky search for generic gravitational-wave bursts and synthesizes the results achieved by the initial generation of interferometric detectors.

DOI: 10.1103/PhysRevD.85.122007 PACS numbers: 95.85.Sz, 04.80.Nn, 07.05.Kf, 95.30.Sf

I. INTRODUCTION

Astrophysical sources of transient gravitational waves (duration of $\lesssim 1$ s) [1] include merging compact binary systems consisting of black holes and/or neutron stars [2,3], core-collapse supernovae [4], neutron star collapse to black holes [5], star-quakes associated with magnetar flares [6] or pulsar glitches [7], cosmic string cusps [8], and other violent events in the Universe. Since many classes of gravitational-wave (GW) bursts cannot be modeled well—if at all—a search for those sources must be sensitive to the widest possible variety of waveforms.

This paper reports on a search for GW bursts occurring during the second joint observation run of the LIGO [9] and Virgo [10] detectors, which took place in 2009–2010. This search makes no prior assumptions on source sky location, signal arrival time, or the waveform itself. Event rate upper limits from long-term searches of this category have been derived with networks of resonant bar detectors with spectral sensitivity limited to around 900 Hz in 1997–2000 [11,12] and in 2005–2007 [13,14]. Networks of interferometric detectors set more stringent upper limits for GW bursts on a wider bandwidth using the LIGO detectors in 2005–2006 [15–17] and during the first joint observation of LIGO and Virgo detectors in 2007 [18].

This second joint LIGO-Virgo search for GW bursts analyzed the frequency band spanning 64–5000 Hz. We achieved a frequency-dependent sensitivity comparable to or better than that of the first joint run, and accumulated ~207 days of observation time interlaced with periods of installing or commissioning major hardware upgrades. Moreover, for the first time a low-latency analysis was run with the goal of providing triggers for electromagnetic follow-ups of candidates by robotic optical telescopes [19], radio telescopes, and the *Swift* satellite [20,21]. In this paper we focus on the final results of the GW stand-alone search, which found no evidence for GW bursts.

This paper is organized as follows. In Sec. II we describe the second joint scientific run: we report on the LIGO and Virgo instrumental upgrades with respect to the first run and on data quality studies. In Sec. III we give a brief overview of the search: the search algorithm, background estimation, the simulations and the calibration uncertainties. The signal models (GW waveforms and source populations) we tested are described in Sec. III C. The results of the search are presented in Sec. IV, and astrophysical implications are discussed in Sec. V. The Appendices provide additional details on data characterization and analysis methods.

II. SECOND LIGO-VIRGO SCIENCE RUN

The network of detectors used in this search comprises the two LIGO 4 km interferometers, denoted "H1" (located in Hanford, WA) and "L1" (Livingston, LA), as

well as the Virgo 3 km interferometer, denoted "V1" (close to Pisa, Italy).[1]

The LIGO detectors operated from July 7, 2009 to October 20, 2010 in their sixth science run (S6). The Virgo detector operated from July 7, 2009 to January 8, 2010 in its second science run (VSR2) and again from August 11 to October 20, 2010 in its third science run (VSR3).

As in the first joint LIGO-Virgo run [18,22], the operation of three differently oriented and widely separated detectors allows for reasonably complete coverage of the sky for at least one gravitational-wave polarization component as well as the recovery of some source characteristics such as sky location [19,23,24].

A. Detector upgrades

Before the beginning of the runs, several detector hardware upgrades were implemented in order to prototype new subsystems planned for the next generation of detectors, referred to as "advanced detectors" [25,26], expected to start observations in 2015. The upgrades of the LIGO detectors for S6 include a higher power 35 W laser, the implementation of a DC readout system, a new output mode cleaner, and an advanced LIGO seismic isolation table [27]. The upgrades of the Virgo detectors were achieved in two steps. For VSR2, Virgo operated with a more powerful laser and a thermal compensation system. Virgo then went offline to install new test masses consisting of mirrors hung from fused silica fibers [28]. Virgo resumed observations in August 2010 with VSR3. Best sensitivities, in terms of noise spectral densities, of the LIGO and Virgo detectors achieved during their second joint run (henceforth defined as S6-VSR2/3), as a function of signal frequency, are shown in Fig. 1.

B. Data quality

To mitigate the consequences of new hardware installations and detector commissioning during this run, significant effort has been made to identify and characterize instrumental or data acquisition artifacts, periods of degraded sensitivity, or an excessive rate of transient noise due to environmental conditions [29]. During such times, the data were tagged with data quality flags (DQFs). Following the same approach used in previous searches [16–18], these DQFs are divided into three categories depending on their impact on the search and on the understanding of the behavior of the detector. A further description of DQF categories is presented in Appendix A.

[1]The 2 km detector at the Hanford site (H2) was decommissioned before the second joint LIGO-Virgo run. During previous runs, the latter detector was mainly used to enforce additional event selection criteria by taking advantage of the special relationship for GW signals from the co-located interferometers H1 and H2.

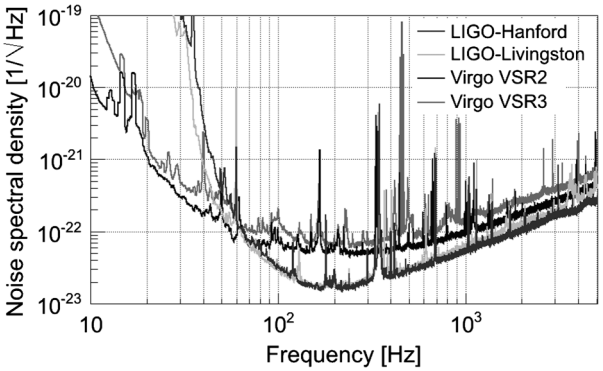

FIG. 1. Noise spectra for the three LSC-Virgo detectors achieved during S6-VSR2/3.

After DQFs have been applied, the total analyzable time for the S6-VSR2/3 run is 242.8 days for H1, 220.2 days for L1, and 187.8 days for V1.

III. SEARCH OVERVIEW

In this analysis, we considered all four available detector network configurations: the three detector network, H1L1V1, and the three combinations of detector pairs, H1L1, H1V1 and L1V1. We decided *a priori* to search for GW bursts in the entire available time of threefold observation and in the remaining exclusive times of the twofold networks. Table I reports the total (nonoverlapping) coincident observation time for each configuration of detectors searched for GW signals. Information about distinct subperiods of the run may be found in Appendix C.

Because of the commissioning breaks and installation activities described in Sec. II, the total observation time is dominated by twofold configurations.

The useful frequency band is limited to 64–5000 Hz by the sensitivity of the detectors and by the valid range of data calibration. For computational reasons, the event search was performed separately in two suitable bands, 64–2048 Hz and 1600–5000 Hz, overlapping to preserve sensitivity to events with spectral power at intermediate frequencies. The analysis of the events (including the tuning of the search) was performed independently on each configuration of detectors and on three sub-bands, namely, 64–200 Hz, 200–1600 Hz and 1600–5000 Hz, by classifying the found events according to their reconstructed central frequency. The motivation for this band splitting is to

TABLE I. Mutually exclusive observation time for each detector configuration after the application of category 2 DQFs (see Appendix A for the definition of data quality flags and their categories).

Network	H1L1V1	H1L1	L1V1	H1V1	Total
Observation time [days]	52.2	84.5	28.9	41.0	206.6

tune the search within event sets of homogeneous glitch behavior.

A. Search algorithm

This search is based on the coherent WaveBurst (cWB) algorithm [29], which has been used since LIGO's fourth science run in various searches for transient GWs [16–18,30].

The cWB analysis is performed in several steps. First, detector data is decomposed into a time-frequency representation and then whitened and conditioned to remove narrow-band noise features. Events are identified by clustering time-frequency pixels with significant energy which is coherent among detectors and characterized using test statistics derived from the likelihood (which is also a measure of the signal energy detected in the network and is calculated as described in [16]). The primary statistics are the network correlation coefficient cc, which is a measure of the degree of correlation between the detectors, and the coherent network amplitude η, which is proportional to the signal-to-noise ratio and is used to rank events within a homogeneous subperiod.

Both of these statistics are described in detail in [16]. The application of the event selection criteria is thoroughly described in [18,31].

Any gravitational-wave candidate event detected by cWB is subject to additional data-quality vetoes based on statistical correlations between the GW data channel and environmental and instrumental auxiliary channels; a significant correlation indicates the event may have been produced by local noise. Further details can be found in Appendix B.

B. Background estimation and search tuning

A sample of "off-source" (background) events is required to determine the selection thresholds to reject noise-induced events contaminating the "on-source" (foreground) measurement. We estimate the distribution of background events by performing the analysis on time-shifted data, typically in $\sim$1 s steps. The shifts minimize the chance of drawing an actual GW into the background sample. To accumulate a sufficient sampling, this shifting procedure is performed hundreds or thousands of times without repeating the same relative time shifts among detectors. Background events corresponding to times which are flagged by data quality studies are discarded, just as an event candidate from the foreground would be.

Because of the different characteristics of the background noise for the various subperiods between commissioning breaks and for the different frequency bands and networks, the thresholds on cc and η are tuned separately for each homogeneous subperiod. Moreover, we consider the action of conditional DQFs (Category 3 DQFs, see Appendix A) on the event significance, by introducing a new ranking scheme which assigns lower significance to events flagged by such DQFs. More details on this procedure are reported in Appendix D.

The thresholds reported in Table VII in Appendix D are selected to require a false alarm rate (FAR) $\lesssim 1/(8\ \mathrm{yr})$ per frequency band. This choice for the FAR threshold corresponds to an overall false alarm probability (FAP) of $\sim$15% when considering the union of all searches performed (network configurations, subperiods, and frequency bands). "On-source" events at higher FAR

TABLE II. Values of $h_{\mathrm{rss}}^{50\%}$ and $h_{\mathrm{rss}}^{90\%}$ (for 50% and 90% detection efficiency at the chosen thresholds of $1/(8\ \mathrm{yr})$ per frequency band), in units of $10^{-22}\ \mathrm{Hz}^{-1/2}$, for linear and elliptical sine-Gaussian waveforms with the central frequency f_0 and quality factor Q. The center two columns are the $h_{\mathrm{rss}}^{50\%}$ for linear and elliptical waveforms during the total S6 period measured for the H1L1V1 network. The rightmost columns report the values of $h_{\mathrm{rss}}^{50\%}$ and $h_{\mathrm{rss}}^{90\%}$ over the whole S6-VSR2/3 for the combined results (i.e. averaged over time) from all the networks.

		H1L1V1		All networks			
		Linear	Elliptical	Linear		Elliptical	
f_0 [Hz]	Q	$h_{\mathrm{rss}}^{50\%}$	$h_{\mathrm{rss}}^{50\%}$	$h_{\mathrm{rss}}^{50\%}$	$h_{\mathrm{rss}}^{90\%}$	$h_{\mathrm{rss}}^{50\%}$	$h_{\mathrm{rss}}^{90\%}$
70	3	18.9	18.0	28.4	311.9	23.2	92.7
70	9	21.5	20.4	31.6	269.4	25.8	91.7
70	100	24.2	21.4	34.4	484.9	27.4	131.9
100	9	10.5	9.6	15.6	156.6	12.6	57.6
153	9	6.7	5.8	10.3	105.4	8.0	35.2
235	3	5.7	5.5	8.5	45.3	7.4	24.4
235	9	5.2	4.9	7.7	39.7	6.6	20.7
235	100	4.6	4.4	7.2	37.6	6.0	19.0
361	9	8.6	8.7	12.4	67.8	11.1	32.7
554	9	8.9	8.4	13.1	69.4	11.1	35.2
849	3	15.1	14.4	20.8	128.7	18.4	56.6
849	9	14.1	13.3	19.7	116.0	17.2	52.0
849	100	12.3	11.4	17.4	88.7	14.8	44.9
1053	9	16.9	17.5	24.2	133.5	21.9	63.9
1304	9	21.1	19.7	30.4	177.9	25.3	78.6
1615	3	41.6		54.5	349.8		
1615	9	35.2		46.3	259.9		
1615	100	28.3		38.8	219.3		
1797	9	26.8		35.4	206.0		
2000	3	41.6		51.8	322.9		
2000	9	30.8		38.7	229.1		
2000	100	27.4		36.0	181.8		
2226	9	36.6		47.2	272.1		
2477	3	51.6		61.2	425.9		
2477	9	44.3		55.2	307.3		
2477	100	34.6		46.3	233.5		
2756	9	44.2		56.8	389.8		
3067	3	74.1		81.7	600.0		
3067	9	64.6		78.0	499.6		
3067	100	41.1		53.8	278.2		
3413	9	65.7		80.0	510.4		
3799	9	81.7		99.3	719.9		

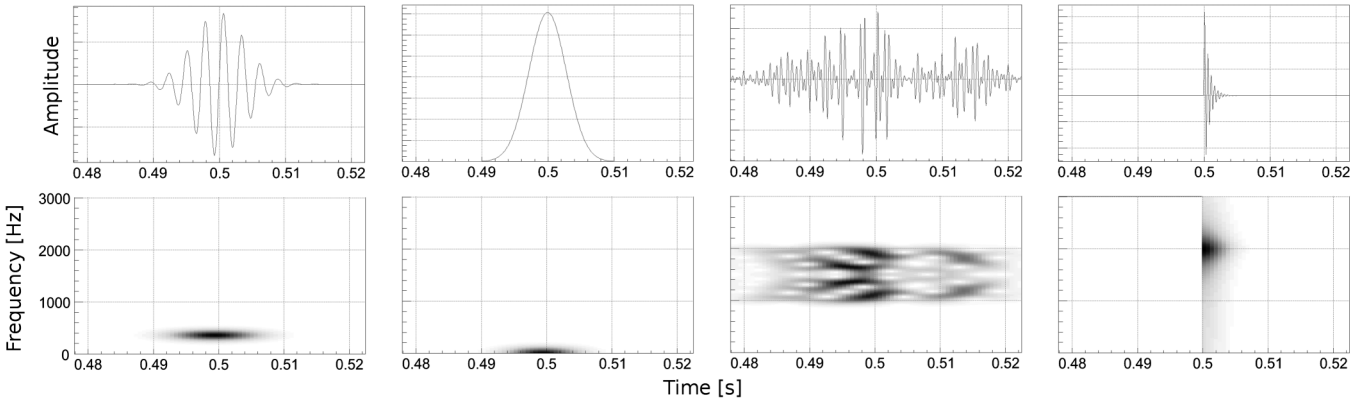

FIG. 2. Representative waveforms injected into data for simulation studies. The top row is the time domain and the bottom row is a time-frequency domain representation of the waveform. From left to right: a 361 Hz $Q = 9$ sine-Gaussian, a $\tau = 4.0$ ms Gaussian waveform, a white noise burst with a bandwidth of 1000–2000 Hz and characteristic duration of $\tau = 20$ ms and, finally, a ring-down waveform with a frequency of 2000 Hz and $\tau = 1$ ms.

are discarded as nonsignificant. Any "on-source" events passing the FAR threshold are instead selected for further follows-up investigations. Namely, we check for any additional evidence about their origin and refine the measurement of their statistical significance (i.e. by performing additional independent time-shifted analyses to increase the statistics of the background estimates). This FAR threshold sets the overall sensitivity of the search.

C. Simulated signals and detection efficiencies

In order to test the sensitivity of our search to gravitational-wave bursts, we add ("inject") various ad-hoc software signals, both polarized and unpolarized, to the detector data and measure the detection efficiencies of the search. The injected waveforms can be parametrized as:

$$\begin{bmatrix} h_+(t) \\ h_\times(t) \end{bmatrix} = A \times \begin{bmatrix} \frac{1+\alpha^2}{2} \\ \alpha \end{bmatrix} \times \begin{bmatrix} H_+(t) \\ H_\times(t) \end{bmatrix}, \tag{3.1}$$

where A is the amplitude, α the ellipticity[2] and $H_{+/\times}$ are the waveforms for the two independent polarizations. In this search, we investigated elliptically polarized signals (i.e. α uniformly chosen in [0, 1]), as well as sets of only linearly or circularly polarized waves (α fixed to 0 or 1, respectively). A variety of GW signal morphologies spanning a wide range of signal durations, frequencies and amplitudes were tested. See Fig. 2 for a sample of representative waveforms from various families and Tables II, III, and IV for the chosen waveform parameters.

The injected waveform families include:

(i) *Sine-Gaussian*:

$$H_+(t) = \exp(-t^2/\tau^2)\sin(2\pi f_0 t) \tag{3.2}$$

$$H_\times(t) = \exp(-t^2/\tau^2)\cos(2\pi f_0 t), \tag{3.3}$$

where $\tau = Q/(\sqrt{2}\pi f_0)$. We consider waveforms of this type with central frequencies f_0 chosen between 70 to 5000 Hz and quality factors $Q = 3, 9, 100$. Sine-Gaussian waveforms with a few cycles are qualitatively similar to signals produced by the mergers of two black holes [2].

(ii) *Gaussian*:

$$H_+(t) = \exp(-t^2/\tau^2) \tag{3.4}$$

$$H_\times(t) = 0, \tag{3.5}$$

where the duration parameter τ is chosen to be one of 0.1, 1.0, 2.5, or 4.0 ms.

(iii) *Ring-down waveforms*:

$$H_+(t) = \exp(-t/\tau)\sin(2\pi f_0 t) \tag{3.6}$$

$$H_\times(t) = \exp(-t/\tau)\cos(2\pi f_0 t). \tag{3.7}$$

We use several central frequencies from 1590 Hz to 3067 Hz, and decay times $\tau = 0.2$ s or $Q = 9$. Ring-downs can occur in the end stages of black hole binary mergers. Longer duration ring-downs are also similar to signals predicted from the excitation of fundamental modes in neutron stars [32].

(iv) *Band-limited white noise signals*: The polarization components are bursts of uncorrelated band-limited white noise, time shaped with a Gaussian profile; H_+ and $H_\times$ have—on average—equal root mean square amplitudes and symmetric shape about the central frequency (see Fig. 2).

(v) *Neutron star collapse waveforms*: For a comparison with previous searches [17,18], we considered numerical simulations by Baiotti *et al.* [5], who modeled neutron star gravitational collapse to a black

[2]For binary sources, the ellipticity is the cosine of the source inclination angle, i.e. the angle between the source rotational axis and the line of sight to Earth.

hole and the subsequent ring-down. As in previous searches, we chose the models D1 (a nearly spherical $1.67M_\odot$ neutron star) and D4 (a $1.86M_\odot$ neutron star that is maximally deformed at the time of its collapse into a black hole) to represent the extremes of the parameter space in mass and spin considered in the aforementioned work. Both waveforms are linearly polarized ($H_\times = 0$) and their emission is peaked at a few kHz.

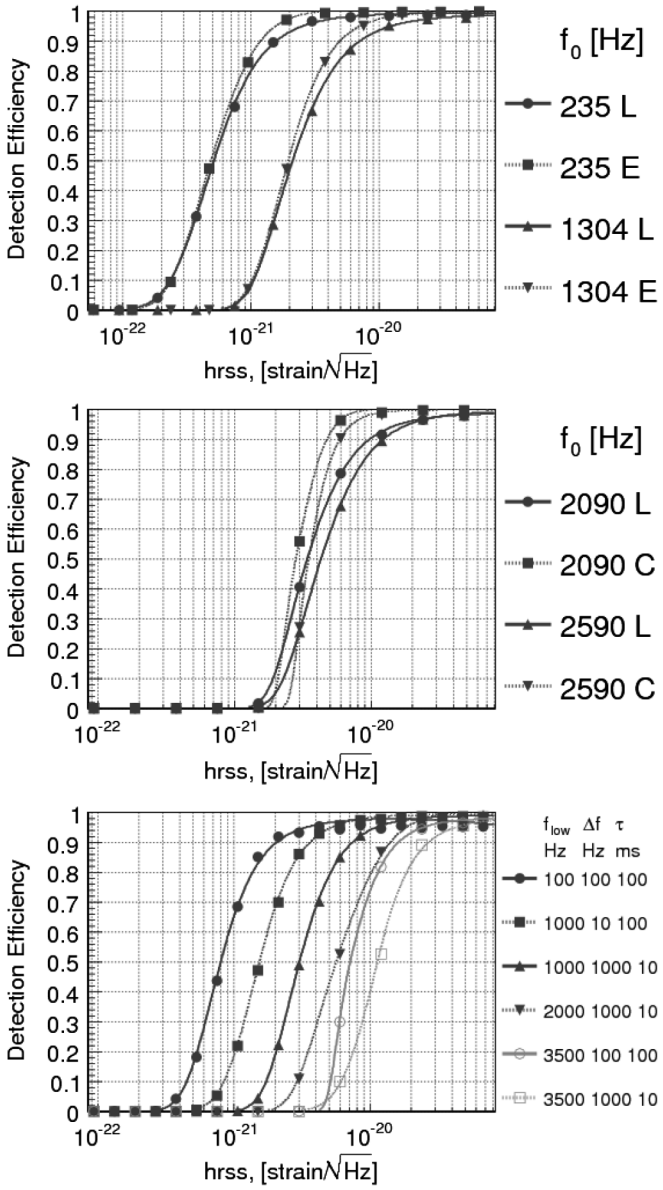

FIG. 3. Detection efficiency for selected waveforms as a function of signal amplitude $h_{\rm rss}$ for the H1L1V1 network. Top: Comparison of detection efficiency for linear (L) and elliptical (E) sine-Gaussians with central frequencies of 235 and 1304 Hz. Middle: Comparison of detection efficiency for linear (L) and circular (C) ring-down signals with frequencies of 2090 and 2590 Hz. Bottom: Detection efficiency for white noise bursts with frequency spanning between 100 and 4500 Hz.

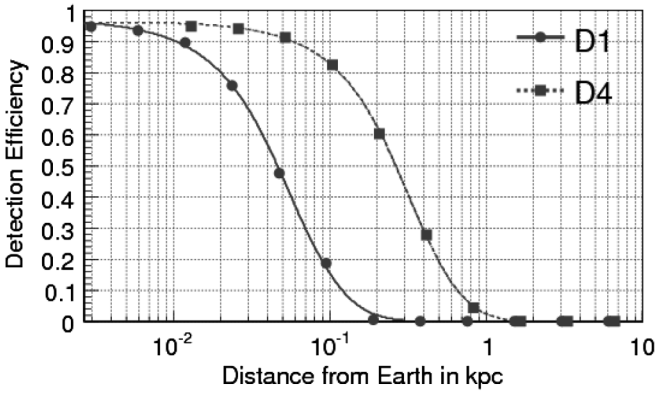

FIG. 4. Efficiency for the H1L1V1 network as a function of distance for the D1 and D4 waveforms predicted by polytropic general-relativistic models of neutron star collapse.

The simulated signals were injected with many amplitude scale factors to trace out the detection efficiency as a function of signal strength. The amplitude of the signal is expressed in terms of the root-sum-square strain amplitude ($h_{\rm rss}$) arriving at the Earth, defined as

$$h_{\rm rss} = \sqrt{\int |h_+(t)|^2 + |h_\times(t)|^2 dt}. \quad (3.8)$$

The signal amplitude at a detector is modulated by the detector antenna pattern functions, expressed as follows:

$$h_{\rm det}(t) = F_+(\Theta, \Phi, \psi)h_+(t) + F_\times(\Theta, \Phi, \psi)h_\times(t), \quad (3.9)$$

where F_+ and $F_\times$ are the antenna pattern functions, which depend on the orientation of the wave front relative to the detector, denoted here in terms of the sky position (Θ, Φ), and on the polarization angle ψ. The sky positions of simulated signals are distributed isotropically and polarization angles are chosen to be uniformly distributed.

The detection efficiency is defined as the fraction of signals successfully recovered using the same selection thresholds and DQFs as in the actual search. The detection efficiency of the search depends on the network

TABLE III. Values of $h_{\rm rss}^{50\%}$ and $h_{\rm rss}^{90\%}$ (for 50% and 90% detection efficiency at the chosen thresholds of $1/(8\ {\rm yr})$ per frequency band), in units of $10^{-22}\ {\rm Hz}^{-1/2}$, for linearly and circularly polarized ring-downs characterized by parameters f and τ.

		All networks			
f	τ	Linear		Circular	
[Hz]	[ms]	$h_{\rm rss}^{50\%}$	$h_{\rm rss}^{90\%}$	$h_{\rm rss}^{50\%}$	$h_{\rm rss}^{90\%}$
2000	1.0	47.3	288	34.8	78.9
2090	200	42.9	218	31.7	66.0
2590	200	52.2	255	39.1	79.5
3067	0.65	91.9	546	72.9	569

TABLE IV. Values of $h_{\rm rss}^{50\%}$ and $h_{\rm rss}^{90\%}$ (for 50% and 90% detection efficiency at the chosen thresholds of $1/(8\ {\rm yr})$ per frequency band), in units of $10^{-22}\ {\rm Hz}^{-1/2}$, for band-limited white noise waveforms characterized by parameters $f_{\rm low}$, Δf, and τ.

$f_{\rm low}$ [Hz]	Δf [Hz]	τ [ms]	H1L1V1 $h_{\rm rss}^{50\%}$	All networks $h_{\rm rss}^{50\%}$	All networks $h_{\rm rss}^{90\%}$
100	100	100	8.1	11.5	91.2
250	100	100	7.5	10.5	43.1
1000	10	100	15.5	22.5	93.6
1000	1000	10	30.5	39.7	130
1000	1000	100	76.8	76.7	492
2000	100	100	35.7	40.3	193
2000	1000	10	55.6	63.1	211
3500	100	100	71.8	90.3	332
3500	1000	10	114	125	371

configuration and the selection cuts used in the analysis. Detection efficiencies for the H1L1V1 network for selected waveforms as a function of signal amplitude $h_{\rm rss}$ and as a function of distance (for the D1 and D4 waveforms from Baiotti *et al.* [5]) are reported in Figs. 3 and 4, respectively. As in the previous joint run, typical sensitivities for this network in terms of $h_{\rm rss}$ for the selected waveforms lie in the range $\sim 5 \times 10^{-22}\ {\rm Hz}^{-1/2}$ to $\sim 1 \times 10^{-20}\ {\rm Hz}^{-1/2}$; typical distances at 50% detection efficiency for neutron star collapse waveforms lie in the range $\sim$50 pc to $\sim$200 pc.

Two convenient characterizations of the sensitivity, the $h_{\rm rss}$ at 50% and 90% detection efficiency ($h_{\rm rss}^{50\%}$ and $h_{\rm rss}^{90\%}$ respectively) are obtained from fitting the efficiency curves and are reported in Tables II, III, and IV for the various families. Notice that the threefold network, H1L1V1, has a better sensitivity than the weighted average over all networks: twofold networks have $\sim 3/4$ of the analyzed live time, but feature a lower sensitivity.

D. Systematic uncertainties

The most relevant systematic uncertainty in the astrophysical interpretation of our results is due to the calibration error on the strain data produced by each detector [33,34]. The effect of calibration systematics on network detection efficiency has been estimated by dedicated simulations of GW signals in which the signal amplitude and phase at each detector is randomly jittered according to the modeled distribution of calibration errors for that detector. The resulting network detection efficiency marginalizes the effect of the systematic uncertainties over the observation time. The main effect can be parametrized as an overall shift of the detection efficiency curves along the signal strength axis. The largest effect over the injected signal waveforms was a 8% increase of the $h_{\rm rss}$ amplitude at fixed detection efficiency.[3] To produce the astrophysical limits shown in Sec. IV, we use the reduced detection efficiency curves obtained by shifting the original fits from Sec. III C and the results in Tables II, III, and IV to 8% larger $h_{\rm rss}$ values.

IV. SEARCH RESULTS

The on-source data have been analyzed following the procedures tuned through the investigation of the off-source background sample, as described in Appendix D. No on-source event has been found above the threshold false alarm rate of once in 8 years per frequency band, and the distribution of on-source events is in agreement with the measured background. Table V lists the five most significant on-source events, as ranked by their inverse false alarm rate (IFAR $= 1/{\rm FAR}$), and taking into account the trial factor due to the three independent searches performed on the disjoint frequency bands.

In addition to the events reported in Table V, this search also detected an on-source event showing a chirping waveform compatible with a compact binary coalescence at a signal-to-noise ratio $\sim$17 in the H1L1V1 network. This event was first identified by a low-latency burst search within minutes of its occurrence on September 16, 2010 and was thoroughly investigated in follow-up studies. Its Inverse False Alarm Rate was estimated at 1.1 yr from comparison with the burst reference background over all trials. After the completion of the analysis, this event was revealed to be a blind hardware injection [35] intended as an end-to-end test of the search for transient signals.[4] As such, the event was removed from the final results.

Upper limits

The new null result can be combined with the previous ones from the latest scientific runs by LIGO and Virgo [16–18] to complete the results achieved by initial generation interferometric detectors.

Assuming a Poisson distribution of astrophysical sources and in the special case of no surviving candidate

[3]Note that, due to an incomplete knowledge of the actuation resonances in [3000, 4000] Hz band of the Hanford detector, very conservative assumptions have been made on calibration uncertainties; the networks including H1 in that frequency band feature a large efficiency loss due to calibration systematics of 24%.

[4]Signal injections were performed via direct excitation of the interferometer mirror test masses. Some of these *hardware injections* were intended to mimic a coherent GW excitation across the network and to provide an end-to-end verification of the detector instrumentation, the data acquisition system and the data analysis software. In addition to those, a *blind injection challenge* was realized consisting of injecting a few simulated signals at times not announced to the collaborations. This was done for the purpose of testing the data analysis pipelines and event validation protocols.

TABLE V. The five most significant events present in the on-source data. IFAR is the inverse false alarm rate [yr] of the event in the entire search, SNR is the signal-to-noise ratio in the whole network, and FAP is the false alarm probability (probability of getting at least as many accidental events as those observed with IFAR $\geq$ the value reported in the first column).

IFAR [yr]	Freq. band	Network	SNR	FAP
0.64	0.2–1.6 kHz	H1L1	11	0.59
0.36	64–200 Hz	H1L1V1	19	0.47
0.28	0.2–1.6 kHz	H1L1	12	0.33
0.19	0.2–1.6 kHz	H1L1	10	0.35
0.17	1.6–5 kHz	H1V1	9	0.24

events, the 90% confidence upper limit is computed as in [36]:

$$R_{90\%} = \frac{2.3}{\sum_k \epsilon_k T_k}, \tag{4.1}$$

where $2.3 = -\log(1\text{–}0.9)$, ϵ_k and T_k are, respectively, the detection efficiency (calculated with selection thresholds as in Sec. III B) and the observation time of the network configuration k, including all available LIGO and LIGO–Virgo observations since November 2005 [16–18].

Figure 5 shows the upper limits on the rate of gravitational-wave bursts at the Earth as a function of signal strength ($h_{\rm rss}$) for selected sine-Gaussian waveforms. The second joint LIGO–Virgo run increases the previous total observation time by roughly 50%, totaling 1.74 yr. Therefore, the resulting 90% upper limit on the rate for strong signals (asymptotic behavior for $\epsilon_k \to 100\%$) decreases from 2.0 to 1.3 yr^{-1} for the 64–1600 Hz band (from 2.2 to 1.4 yr^{-1} for the band above 1.6 kHz).

The results can also be interpreted as limits on the rate density of GW bursts (number per year and per Mpc^3) assuming a standard-candle source, isotropically distributed, as previously reported in [18]. Denoting by h_0^2 the average value of the GW squared amplitude $h_{\rm rss}^2$ at a fiducial distance r_0 from the source, the energy converted to GWs is

$$E_{\rm GW} = \frac{\pi^2 c^3}{G} r_0^2 f_0^2 h_0^2, \tag{4.2}$$

where f_0 is the central frequency of GW emission.

Considering a population of standard-candle sources randomly oriented with respect to the Earth and at a distance r_0, we can interpret the h_0^2 as the average GW squared amplitude impinging on the Earth (e.g. averaged over source parameters such as inclination angle). Equation (4.2) can then be used to estimate $h_0(E_{\rm GW}, f_0, r_0)$ and, in particular, sets the inverse proportionality between the average $h_{\rm rss}$ at Earth and source distance r: $hr = h_0 r_0$. Assuming a uniform distribution in the sky and in time of these standard-candle sources, the expected rate of detections is

$$\begin{aligned} N_{\rm det} &= 4\pi \mathcal{R} T \int_0^\infty dr r^2 \epsilon(r) \\ &= 4\pi \mathcal{R} T (h_0 r_0)^3 \int_0^\infty dh h^{-4} \epsilon(h), \end{aligned} \tag{4.3}$$

where $\mathcal{R}$ is the rate density of the standard-candle sources, T the overall observation time, and $\epsilon(h)$ the detection efficiency as measured by our simulations.

Hence, the 90% confidence upper limit on rate density $\mathcal{R}$ of such standard-candle sources is

$$\mathcal{R}_{90\%} = \frac{2.3}{4\pi T (h_0 r_0)^3 \int_0^\infty dh h^{-4} \epsilon(h)}. \tag{4.4}$$

The resulting $\mathcal{R}_{90\%}$ is dominated by the part of the detection efficiency curve at small GW amplitude h. Because of

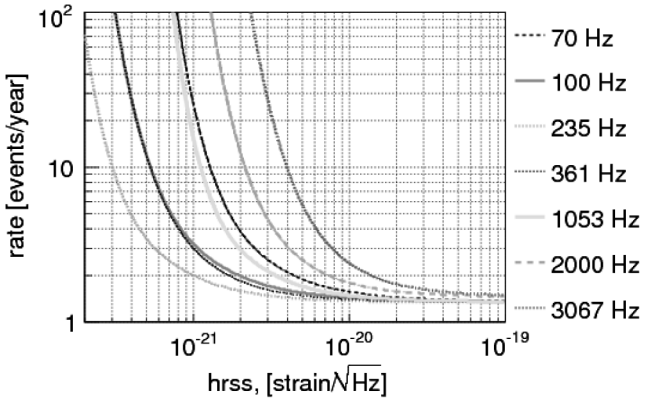

FIG. 5. Upper limits at 90% confidence on the rate of gravitational-wave bursts at Earth as a function of $h_{\rm rss}$ signal amplitude for selected sine-Gaussian waveforms with $Q = 9$. The results include all the LIGO and LIGO–Virgo observations since November 2005.

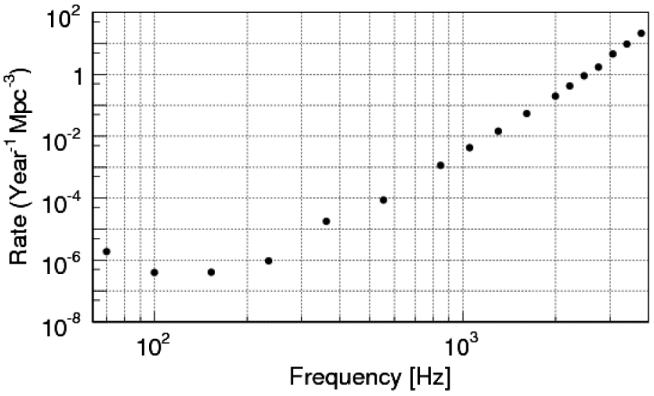

FIG. 6. Rate limit per unit volume for standard-candle sources at the 90% confidence level for a linearly polarized sine-Gaussian standard-candle with $E_{\rm GW} = M_\odot c^2$. Within an accuracy of a few percent, the same numerical results hold also for sources emitting circularly polarized GWs, which would subsequently appear elliptically polarized at the Earth. In this Figure, all LIGO and LIGO–Virgo observations since November 2005 have been combined together.

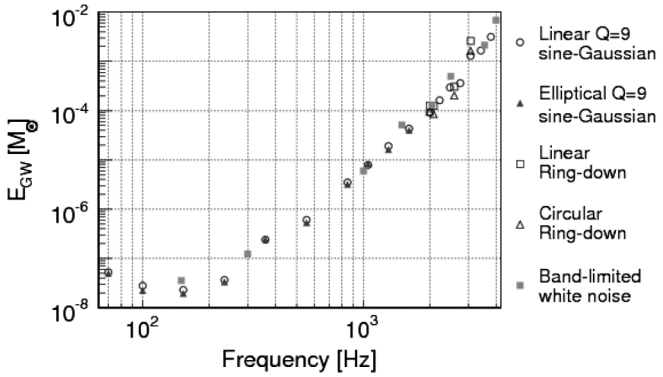

FIG. 7. Typical GW energy in solar masses at 50% detection efficiency for standard-candle sources emitting at 10 kpc for the waveforms listed in Tables II, III, and IV considering the H1L1V1 network and the LIGO-Virgo observations since July 2009.

the relative orientations of the LIGO-Virgo detectors, detection efficiency curves for linearly polarized sine-Gaussian waveforms are approximately the same of those for elliptically polarized ones; the numerical values of $\mathcal{R}_{90\%}$ are close within a few percent for both source models.

Figure 6 shows the rate density upper limits of sources as a function of frequency. This result can be interpreted in the following way: given a standard-candle source with a characteristic frequency f and energy $E_{\rm GW}$, the corresponding rate limit is $\mathcal{R}_{90\%}(f) \times (M_\odot c^2/E_{\rm GW})^{3/2}$ yr^{-1} Mpc^{-3}.

The typical GW energy in units of solar masses for LIGO-Virgo observation is shown in Fig. 7 computed with Eq. (4.2) using the measured $h_{\rm rss}$ at 50% detection efficiency for the tested waveforms assuming a standard-candle source emitting at a distance of 10 kpc. The mass scales with the square of the fiducial distance and the results are robust over the very wide class of waveforms tested. As expected, the GW energy is strongly dependent on the spectral sensitivity of the network, with a negligible dependence on the specific waveform characteristics.

V. SUMMARY AND DISCUSSION

This paper reports the results achieved by the LIGO and Virgo detectors in the search for GW transients of duration $\lesssim 1$ s, without assumptions on the signal waveform, polarization, direction or arrival time.

Three detectors were operating at the Hanford, Livingston and Pisa sites during the second joint observation of LIGO and Virgo in 2009–2010. The detectors implemented hardware upgrades in order to prototype new subsystems planned for the upcoming advanced detectors. The resulting sensitivities to GWs were comparable to those achieved during the first LIGO-Virgo run. The main contribution of the second run is a 50% increase in accumulated observation time.

No event candidates were found in this search. We set better upper limits on the rate of gravitational-wave bursts at Earth and on the rate density of burst sources per unit time and volume. These limits combine all available information from the LIGO–Virgo joint runs and set the state-of-the-art on all-sky searches for transient gravitational waves of short duration.

The reported $h_{\rm rss}$ amplitude of the GW at Earth can be converted into the energy emitted by a source at some fiducial distance assuming a simple model as in Eq. (4.2). For example, the energy emitted in gravitational waves in units of solar masses at a distance of 10 kpc and considering measured $h_{\rm rss}$ at 50% detection efficiency (Table II) is $\simeq 2.2 \cdot 10^{-8} M_\odot$ for signal frequencies near 150 Hz ($5.6 \cdot 10^{-2} M_\odot$ at 16 Mpc). These GW energies, though obviously depending on the signal frequency, are approximately constant over different polarization models of the GW emission, including linearly polarized sources, circularly polarized sources and unpolarized emission with random polarization amplitudes (see Tables II, III, and IV).

The long baseline interferometric detectors LIGO and Virgo are currently being upgraded to their advanced configurations, and the next joint observation is planned for 2015. Another advanced detector, LCGT [37,38], is being built in Japan, and there are proposals to realize an additional advanced LIGO detector outside the USA. These advanced detectors should achieve strain sensitivities a factor of 10 better than the first-generation detectors. For example, at design sensitivity these detectors should detect a typical core-collapse supernova anywhere in the galaxy [39] and will be able to put constraints on extreme scenarios for core-collapse supernovae within the local group [4,40]. Other possible short duration sources, such as the merger of very high mass stellar black hole binaries, could be visible at distances exceeding 1 Gpc. During advanced detector observations, gravitational-wave detections are predicted to occur on a regular basis [41], thus greatly expanding the field of gravitational-wave astrophysics.

ACKNOWLEDGMENTS

The authors gratefully acknowledge the support of the United States National Science Foundation for the construction and operation of the LIGO Laboratory, the Science and Technology Facilities Council of the United Kingdom, the Max-Planck-Society and the State of Niedersachsen/Germany for support of the construction and operation of the GEO 600 detector, and the Italian Istituto Nazionale di Fisica Nucleare and the French Centre National de la Recherche Scientifique for the construction and operation of the Virgo detector. The authors also gratefully acknowledge the support of the research by these agencies and by the Australian Research Council, the Council of Scientific and Industrial Research of India, the Istituto Nazionale di Fisica Nucleare of Italy, the Spanish Ministerio de Educación y Ciencia, the Conselleria

d'Economia Hisenda i Innovació of the Govern de les Illes Balears, the Foundation for Fundamental Research on Matter supported by the Netherlands Organisation for Scientific Research, the Polish Ministry of Science and Higher Education, the FOCUS Programme of Foundation for Polish Science, the Royal Society, the Scottish Funding Council, the Scottish Universities Physics Alliance, the National Aeronautics and Space Administration, the Carnegie Trust, the Leverhulme Trust, the David and Lucile Packard Foundation, the Research Corporation, and the Alfred P. Sloan Foundation. This document has been assigned LIGO Laboratory document number LIGO-P1100118-v16.

APPENDIX A: DATA QUALITY FLAGS

DQFs are intended to indicate periods of data taking which suffer from environmental and instrumental effects inducing noise into the data [29]. We followed the DQF strategy used in previous searches [16–18], organizing DQFs into 3 categories. The different categories reflect the level of understanding of the detectors' performances as well as of the relation between disturbances in the data set and environmental or instrumental causes.

Category 1 DQFs mark segments of time (typically more than tens of seconds) when disturbances make analysis unfeasible. Data segments remaining after their application are used in the analysis.

Category 2 DQFs are connected to well-understood short duration (typically a few seconds) periods of noise transients. Data segments flagged by this category can be used for data conditioning and noise property estimation, but events emerging from these periods are discarded as very likely originating from the detector environment.

Finally, Category 3 DQFs denote periods that are only weakly correlated to environmental and instrumental monitors. Such cuts are not reliable enough to be used as unconditional cuts. When applied to events generated by the search algorithm, they would reject a significant fraction (in extreme cases up to 15–20%) of data. Their use is limited to significance calculations using the modified inverse false alarm rate (MIFAR) statistic (see Appendix D).

APPENDIX B: EVENT-BY-EVENT VETOES

Often, GW candidate events identified in the on-source time can be linked to disturbances propagating through the detector from the environment or within the detector itself. Our procedure for identifying such *event-by-event* vetoes in S6 and VSR2/3 follows that used in S5 and VSR1 [16,18]. The GW channel and a large number of auxiliary channels are processed with the Kleine-Welle [42] algorithm, which looks for excess power transients. A hierarchical method [43] is used to rank the statistical relationship between the transients found in the auxiliary channels and those found in the detector output. Based on these rankings, vetoes are defined for suspected noise events. Another veto used was based on significant statistical association of events observed in the GW channel and the auxiliary channels [44].

An additional set of Category 3 vetoes [45] are applied to events emerging from networks including Virgo; vetoes from this set are based on detector readout channels which are known to be insensitive to gravitational waves.

Procedurally, the event-by-event vetoes are applied with the same conditions as their corresponding category of data quality flags described in Appendix A.

APPENDIX C: DETECTOR NETWORKS AND LIVE TIMES

The total observation time for the analysis has been divided into four subperiods (labeled A, B, C and D), separated by planned commissioning and upgrade breaks which changed the performance of the detectors. Table VI shows the observation time of each network configuration after the application of Category 1 and 2 DQFs. These times are not overlapping. During the period from January to June 2010 (subperiod C), Virgo did not participate in the run because of hardware upgrades.

APPENDIX D: MODIFIED INVERSE FALSE ALARM RATE

We introduce the MIFAR to account for the effect of Category 3 DQFs on the background.

Category 3 DQFs indicate a weak statistical correlation of the GW data with environmental and instrumental noise sources, and thus were used only as a cautionary tag when examining an event in candidate follow-ups. Moreover, the effectiveness of these flags is not constant between different subperiods, network configurations or frequency bands. The use of Category 3 data quality as a tag allows us to produce two sets of events: the "raw" set (polluted to some extent by noise glitches) and the subset of those events that are not tagged, the "clean" set (with reduced observation time).

TABLE VI. Observation time for each detector configuration after application of Category 1 and 2 DQFs for the four subperiods A, B, C, and D. For period A, the observation time of the H1L1 network after subtracting the H1L1V1 observation time is negligible ($\sim$ 1 day). During period C, Virgo did not participate in the run.

detectors	A [days]	B [days]	C [days]	D [days]	TOT [days]
H1L1V1	10.6	16.7	-	24.9	52.2
H1L1	-	6.2	51.4	26.8	84.5
L1V1	10.2	10.7	-	8.1	28.9
H1V1	12.6	21.3	-	7.1	41.0
TOT	33.4	54.8	51.4	66.9	206.6

In order to account for the difference in background distributions when assessing the significance of candidate GW events from the raw and clean sets, we use the following procedure:

(1) Within each homogeneous analysis (same detector's configuration, same tuning of analysis, same frequency band), we rank events from the two sets separately by their coherent network amplitude η; i.e., if the event candidate is flagged by Category 3 data quality, it is ranked against the raw set of events, otherwise it is ranked against the clean set.
(2) Each event is then assigned a MIFAR as the inverse of the rate of higher-ranked background events in that set, i.e. the MIFAR is the IFAR of the event considering only that set.
(3) We merge the events from the raw and clean sets into a single list, sorted by the MIFAR. For events with equal MIFAR the one with larger η is ranked higher. This ranking is performed separately for each homogeneous analysis.
(4) According to this merged ranking, we measure the IFAR of the events as the rate of the corresponding background event with equal MIFAR. This measured IFAR is used as our "universal" ranking for all events in all analyses.
(5) The final IFAR of any event over the entire search is just $1/3$ of the value estimated in the previous step because of the trials factor: three independent analyses have been performed for the three disjoint frequency bands. No contribution to the trials factor comes from the analyses of different detectors' configuration since these were performed on nonoverlapped observation times.

TABLE VII. Thresholds per network, subperiod and frequency band for the homogeneous analyses performed. The threshold η_1 is applied to the events in the raw set (those in coincidence with a Category 3 DQF) and η_2 is applied to events in the clean set (not in coincidence with a DQF). These thresholds have been selected in order to ensure a IFAR ≥ 8 yr.

		Frequency band [Hz]								
Network		64–200			200–2000			2000–5000		
		cc	η_1	η_2	cc	η_1	η_2	cc	η_1	η_2
H1L1V1	A	0.70	5.9	-	0.70	6.0	-	0.65	4.6	-
	B	0.60	6.5	6.5	0.60	4.6	3.9	0.60	3.9	-
	D	0.60	6.7	4.7	0.60	4.5	4.3	0.60	4.7	4.4
H1L1	A	0.65	32.0	-	0.65	7.4	-	0.65	5.8	-
	B	0.60	8.5	8.1	0.60	5.5	5.5	0.60	4.7	-
	C	0.60	8.8	6.4	0.60	6.4	5.5	0.60	4.6	-
	D	0.60	8.9	8.9	0.60	12.9	9.9	0.60	4.7	4.6
					0.60	5.1	4.8			
L1V1	A	0.65	16.8	-	0.65	6.0	-	0.65	5.5	-
	B	0.60	5.8	5.8	0.60	6.4	5.0	0.60	4.6	-
	D	0.60	17.0	17.0	0.60	10.3	10.3	0.60	7.3	6.9
H1V1	A	0.65	10.2	-	0.65	5.2	-	0.65	5.4	-
	B	0.60	6.3	5.3	0.60	5.2	5.0	0.60	4.4	-
	D	0.60	9.1	9.0	0.60	6.1	6.1	0.60	6.3	6.2

In each homogeneous analysis, setting a threshold on IFAR corresponds to two thresholds on η, one for the raw set and one for the clean data set. Table VII reports the selected thresholds. These thresholds were tuned using the background and injection events, without considering the on-source events to avoid bias in candidate selection.

[1] C. Cutler and K. S. Thorne, in *Proceedings of GR16*, edited by N. T. Bishop and S. D. Maharaj (World Scientific, Singapore, 2002).
[2] F. Pretorius, in *Physics of Relativistic Objects in Compact Binaries: From Birth to Coalescence*, edited by M. Colpi , P. Casella, V. Gorini, U. Moschella, and A. Possenti. (Springer-Verlag, Berlin and Canopus Publishing Limited, Bristol, UK, 2009).
[3] Z. B. Etienne, J. A. Faber, Y. T. Liu, S. L. Shapiro, K. Taniguchi, and T. W. Baumgarte, Phys. Rev. D **77**, 084002 (2008).
[4] C. D. Ott, Classical Quantum Gravity **26**, 063001 (2009).
[5] L. Baiotti, I. Hawke, and L. Rezzolla, Classical Quantum Gravity **24**, S187 (2007).
[6] S. Mereghetti, Astron. Astrophys. Rev. **15**, 225 (2008).
[7] N. Andersson and G. L. Comer, Phys. Rev. Lett. **87**, 241101 (2001).
[8] T. Damour and A. Vilenkin, Phys. Rev. D **64**, 064008 (2001).
[9] B. Abbott *et al.* (LIGO Scientific Collaboration), Rep. Prog. Phys. **72**, 076901 (2009).
[10] F. Acernese *et al.*, J. Phys. Conf. Ser. **32**, 223 (2006).
[11] Z. A. Allen *et al.* (International Gravitational Event Collaboration), Phys. Rev. Lett. **85**, 5046 (2000).
[12] P. Astone *et al.* (International Gravitational Event Collaboration), Phys. Rev. D **68**, 022001 (2003).
[13] P. Astone *et al.* (IGEC-2 Collaboration), Phys. Rev. D **76**, 102001 (2007).
[14] P. Astone *et al.* (IGEC-2 Collaboration), Phys. Rev. D **82**, 022003 (2010).
[15] B. Abbott *et al.* (LIGO Scientific Collaboration), Classical Quantum Gravity **24**, 5343 (2007).
[16] B. P. Abbott *et al.* (LIGO Scientific Collaboration), Phys. Rev. D **80**, 102001 (2009).

[17] B. P. Abbott *et al.* (LIGO Scientific Collaboration), Phys. Rev. D **80**, 102002 (2009).
[18] J. Abadie *et al.* (LIGO Scientific Collaboration and Virgo Collaboration), Phys. Rev. D **81**, 102001 (2010).
[19] J. Abadie *et al.* (The LIGO Scientific Collaboration and Virgo Collaboration), arXiv:1109.3498 [Astron. Astrophys. (to be published)].
[20] N. Gehrels *et al.*, Astrophys. J. **611**, 1005 (2004).
[21] N. Gehrels *et al.*, Astrophys. J. **621**, 558 (2005).
[22] J. Abadie *et al.* (LIGO Scientific Collaboration and Virgo Collaboration), Phys. Rev. D **82**, 102001 (2010).
[23] S. Klimenko, G. Vedovato, M. Drago, G. Mazzolo, G. Mitselmakher, C. Pankow, G. Prodi, V. Re, F. Salemi, and I. Yakushin, Phys. Rev. D **83**, 102001 (2011).
[24] B. F. Schutz, Classical Quantum Gravity **28**, 125023 (2011).
[25] G. M. Harry (The LIGO Scientific Collaboration), Classical Quantum Gravity **27**, 084006 (2010).
[26] F. Acernese *et al.*, Report No. VIR0027A09, 2009, URL https://pub3.ego-gw.it/itf/tds/file.php?callFile=VIR-0027A-09.pdf.
[27] R. Adhikari, P. Fritschel, and S. Waldman, Tech. Report No. LIGO-T060156-v1, LIGO Project 2006, URL https://dcc.ligo.org/cgi-bin/DocDB/ShowDocument?docid=7384.
[28] M. Lorenzini, Classical Quantum Gravity **27**, 084021 (2010).
[29] S. Klimenko, I. Yakushin, A. Mercer, and G. Mitselmakher, Classical Quantum Gravity **25**, 114029 (2008).
[30] B. Abbott *et al.*, Classical Quantum Gravity **25**, 245008 (2008).
[31] C. Pankow, S. Klimenko, G. Mitselmakher, I. Yakushin, G. Vedovato, M. Drago, R. A. Mercer, and P. Ajith, Classical Quantum Gravity **26**, 204004 (2009).
[32] O. Benhar, V. Ferrari, and L. Gualtieri, Phys. Rev. D **70**, 124015 (2004).
[33] J. Abadie *et al.* (LIGO Scientific Collaboration), Nucl. Instrum. Methods Phys. Res., Sect. A **624**, 223 (2010).
[34] T. Accadia *et al.* (Virgo Collaboration), Classical Quantum Gravity **28**, 025005 (2011).
[35] Open web page, URL http://www.ligo.org/science/GW100916/index.php.
[36] P. J. Sutton, Classical Quantum Gravity **26**, 245007 (2009).
[37] T. Uchiyama *et al.*, Classical Quantum Gravity **21**, S1161 (2004).
[38] K. Kuroda, Classical Quantum Gravity **27**, 084004 (2010).
[39] K. N. Yakunin *et al.*, Classical Quantum Gravity **27**, 194005 (2010).
[40] C. L. Fryer and K. C. B. New, Living Rev. Relativity **14**, 1 (2011).
[41] J. Abadie *et al.* (LIGO Scientific Collaboration and Virgo Collaboration), Classical Quantum Gravity **27**, 173001 (2010).
[42] S. Chatterji, L. Blackburn, G. Martin, and E. Katsavounidis, Classical Quantum Gravity **21**, S1809 (2004).
[43] J. R. Smith, T. Abbott, E. Hirose, N. Leroy, D. MacLeod, J. McIver, P. Saulson, and P. Shawhan, Classical Quantum Gravity **28**, 235005 (2011).
[44] T. Isogai *et al.*, J. Phys. Conf. Ser. **243**, 012005 (2010).
[45] T. Ballinger, Classical Quantum Gravity **26**, 204003 (2009).